Explaining $g_\mu - 2$ and $R_{K^{(*)}}$ using the light mediators of $U(1)_{T3R}$

Bhaskar Dutta,[1,*] Sumit Ghosh,[1,†] Peisi Huang,[2,‡] and Jason Kumar[3,§]

[1]*Mitchell Institute for Fundamental Physics and Astronomy, Department of Physics and Astronomy, Texas A&M University, College Station, Texas 77843, USA*

[2]*Department of Physics and Astronomy, University of Nebraska, Lincoln, Nebraska 68588, USA*

[3]*Department of Physics and Astronomy, University of Hawaii, Honolulu, Hawaii 96822, USA*

(Received 28 May 2021; accepted 23 December 2021; published 11 January 2022)

Scenarios in which right-handed light Standard Model fermions couple to a new gauge group, $U(1)_{T3R}$, can naturally generate a sub-GeV dark matter candidate. But such models necessarily have large couplings to the Standard Model, generally yielding tight experimental constraints. We show that the contributions to $g_\mu - 2$ from the dark photon and dark Higgs largely cancel out in the narrow window where all the experimental constraints are satisfied, leaving a net correction that is consistent with recent measurements from Fermilab. These models inherently violate lepton universality, and UV completions of these models can include quark flavor violation that can explain $R_{K^{(*)}}$ anomalies as observed at the LHCb experiment after satisfying constraints on $\mathrm{Br}(B_s \to \mu^+\mu^-)$ and various other constraints in the allowed parameter space of the model. This scenario can be probed by FASER, SeaQuest, SHiP, LHCb, Belle, etc.

DOI: 10.1103/PhysRevD.105.015011

I. INTRODUCTION

The $g_\mu - 2$ anomaly has been one of the most promising signals of possible new physics beyond the Standard Model (SM) [1–8]. There are a variety of new physics scenarios which can potentially explain this anomaly and which typically rely either on new heavy particles with a large coupling to muons or light particles with a very small coupling to muons. But there is an interesting scenario in which right-handed muons and other first- or second-generation fermions are charged under a new gauge group, $U(1)_{T3R}$ [9–11]. In this scenario, the symmetry-breaking scale of $U(1)_{T3R}$ ($\sim\mathcal{O}(10\ \mathrm{GeV})$) naturally feeds into the light SM fermion mass parameters, as well as the dark sector, yielding a sub-GeV dark matter candidate. But the blessing is also a curse, as in this scenario the mediators inherently have a large coupling to the SM, resulting in tight experimental constraints, and a typically very large correction to $g_\mu - 2$. There is only a small window in which the model is not ruled out by current laboratory, astrophysical and cosmological observables. But within this narrow window, there is a region of parameter space in which the dark Higgs (ϕ') and dark photon (A') contributions to $g_\mu - 2$ largely cancel, yielding a net contribution to $g_\mu - 2$, which is consistent with the newest measurement from Fermilab.

The combined data of Fermilab [12] and BNL [1] increases the tension between the experimental value and the theoretical prediction [3–8,13–28] to 4.2σ level. This is given by

$$\Delta a_\mu = a_\mu^{\mathrm{exp}} - a_\mu^{\mathrm{th}} = (2.52 \pm 0.59) \times 10^{-9}. \qquad (1)$$

The tension is less significant as claimed in a recent lattice calculation [29] which needs to be investigated further [30–32].

The mass terms for fermions charged under $U(1)_{T3R}$ arise from nonrenormalizable operators at the electroweak symmetry-breaking scale. A variety of UV completions of these models are possible, which generically permit quark flavor-violating processes involving heavy particles. On the other hand, since $U(1)_{T3R}$ couples to one complete generation, it necessarily induces lepton flavor nonuniversality through processes mediated by light mediators. These processes together can generate anomalous lepton nonuniversality in b decays, which can potentially explain the recently observed $R_{K^{(*)}}$ anomalies [33–35]. These anomalies are very clean observables since they are devoid of hadronic uncertainties. Very recently, using the full run-1 and run-2 dataset, the LHCb collaboration updated the R_K result which now shows a 3.1σ deviation from the SM [35]. The full data analysis shows

*dutta@physics.tamu.edu
†ghosh@tamu.edu
‡peisi.huang@unl.edu
§jkumar@hawaii.edu

$$R_K = 0.846^{+0.042}_{-0.039}(\text{stat})^{+0.013}_{-0.012}(\text{syst}), \quad (2)$$

where the SM calculation yields $R_K = 1.00 \pm 0.01$ [36–38].

Since the $g_\mu - 2$ excess and the $R_{K^{(*)}}$ anomalies are indications of nonuniversality in the muon sector, it would be interesting to accommodate both of them in the context of a model (for recent work, see [39,40]). Such a model, however, can be constrained by various other experimental data. For example, the CCFR constraint on $\nu_\mu N \to \nu_\mu N \mu^+ \mu^-$ interaction [41] makes it difficult for a model to explain both anomalies [42,43]. Measurement of $\text{Br}(B \to K^{(*)} \nu\nu)$ also restrict the parameter space. Both these neutrino related measurements constrain models which utilize left-handed muons to solve the $R_{K^{(*)}}$ puzzles. Additionally, the measurements of $\text{Br}(B_s \to \mu^+\mu^-)$ restrict the parameter space of such models. In the context of the $U(1)_{T3R}$ model, where the new gauge boson does not couple to the left-handed neutrino, we will show how both anomalies can be accommodated after satisfying various experimental data including the recent muon $g-2$ result. We also show the predictions for a few more B decay observables which can test this model with more data, new measurements and improved theoretical understanding of form factors.

A good way to probe the allowed parameter space of this scenario experimentally is at beam dump experiments with a displaced detector, where one can search for the decays of the long-lived dark photon to e^+e^-. The difficulty is that, because these models have a relatively large coupling to the Standard Models, the decay length of the A' tends to be shorter than typically expected; although it exits the immediate interaction region, it often will decay before reaching many displaced detectors. Thus there are regions of parameter space ($m_{\phi'} \sim 70$–90 MeV, $m_{A'} \sim 60$–200 MeV) in which the measured value of $g_\mu - 2$ can be explained, and which lie just beyond current bounds from U70/NuCal [42,44,45]. Portions of this region can be probed by FASER [46–50], SeaQuest [51,52], and SHiP [53,54]. There is a portion of this parameter space ($m_{A'} > 110\,\text{MeV}$) which cannot be explored by even these experiments.

Alternatively, if the A' decays invisibly, then there is a region of parameter space ($m_{\phi'} \sim 95$–102 MeV, $m_{A'} \sim 10$–30 MeV) in which scenario will again evade all constraints from laboratory experiments and cosmological observables while also yielding a prediction for $g_\mu - 2$ which is consistent with the experiment. Interestingly, this scenario can also potentially explain an excess event rate seen by the COHERENT experiment, and this mass range can be probed by the upcoming NA-64μ and LDMX-M^3 experiments.

The plan of this paper is as follows. In Sec. II, we review the $U(1)_{T3R}$ model and the contribution to $g_\mu - 2$. In Sec. III, we discuss constraints on this scenario, and identify the regions of parameter space which are allowed, and the experiments which may further constrain this scenario. In Sec. IV, we discuss the explanations of the $R_{K^{(*)}}$ anomalies in the allowed parameter space of the model and list various predictions. In Sec. V, we conclude.

II. THE MODEL AND $g_\mu - 2$

We consider the scenario in which the right-handed μ, ν, u and d are charged under $U(1)_{T3R}$, with up-type and down-type fermions having opposite sign charges (± 2). In this scenario, all gauge anomalies automatically cancel. Note, it is technically natural [55] for the charged lepton and either the up-type or down-type quark charged under $U(1)_{T3R}$ to be mass eigenstates. The details of this model are described in [9–11], and are reproduced in the Appendix.

$U(1)_{T3R}$ is spontaneously broken to a parity by the condensation of the scalar field ϕ. We denote by $V = \langle\phi\rangle$ the vacuum expectation value of ϕ, while the dark Higgs ϕ' is the real field which denotes an excitation away from the vacuum expectation value (vev). The dark photon A' then gets a mass given by $m_{A'}^2 = 2g_{T3R}^2 V^2$, where g_{T3R} is the coupling of $U(1)_{T3R}$.

Because the right-handed muon is charged under $U(1)_{T3R}$, while the left-handed muon is not, the muon mass is protected by $U(1)_{T3R}$. As a result, in the low-energy effective field theory (below the scale of electroweak symmetry breaking), ϕ couples to the muon as $\lambda_\mu \phi \bar{\mu}\mu$. If we define $\phi = V + (1/\sqrt{2})\phi'$, then we find $m_\mu = \lambda_\mu V$; if we choose $V = \mathcal{O}(10\,\text{GeV})$, then the effective Yukawa coupling λ_μ is not unnaturally small. The dark Higgs then couples to muons with a coupling $m_\mu/\sqrt{2}V$.

The dark sector also includes a Dirac fermion η with charge 1 under $U(1)_{T3R}$. This fermion can get a Majorana mass term through a coupling to ϕ; if this is larger than the Dirac mass, then one is left with two dark sector Majorana fermions, $\eta_{1,2}$ with masses proportional to V and a small mass splitting. These fermions also couple to ϕ' and A'. The $\eta_{1,2}$ are the only particles which are odd under the surviving parity, and the lightest of these is a dark matter candidate with a mass which is naturally sub-GeV.

The new fields added in this model are A', ϕ', $\eta_{1,2}$ and ν_R. We assume that the sterile neutrino ν_S is mostly ν_R, with only a very small mixing with left-handed neutrinos. If the sterile neutrino is reasonably light, it can be relevant in formulating constraints on this scenario. For simplicity, we will assume that it is moderately heavy, and plays little role in these constraints.

We thus see that, once we specify V, $m_{A'}$ and $m_{\phi'}$, the coupling of the dark photon and the dark Higgs to the muon are fixed. We will set $V = 10$ GeV, following [9], and consider the correction to the muon magnetic moment as a function of $m_{A'}$ and $m_{\phi'}$.

The muon anomalous magnetic moment will receive corrections arising from diagrams in which either ϕ' or A'

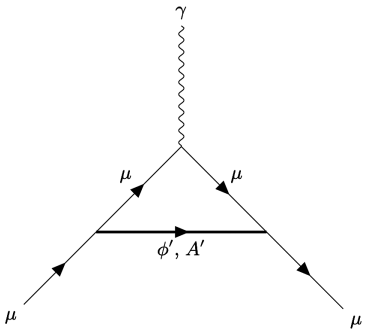

FIG. 1. One-loop ϕ'/A' contribution to g_μ-2.

run in the loop (see Fig. 1). The correction to $a_\mu = (g_\mu - 2)/2$ due to one-loop diagrams involving A' and ϕ' is given by [56]

$$\begin{aligned}\Delta a_\mu &= \frac{m_\mu^4}{16\pi^2 V^2}\int_0^1 dx \frac{(1-x)^2(1+x)}{(1-x)^2 m_\mu^2 + x m_{\phi'}^2} \\ &\quad + \frac{m_\mu^2}{16\pi^2 V^2}\int_0^1 dx \frac{x(1-x)(x-2)m_{A'}^2 - x^3 m_\mu^2}{x^2 m_\mu^2 + (1-x)m_{A'}^2}, \\ &= (6.98\times 10^{-7})\left(\frac{V}{10\ \text{GeV}}\right)^{-2}(C_{\phi'} - C_{A'}), \end{aligned} \tag{3}$$

where

$$\begin{aligned} C_{\phi'} &= \int_0^1 dx \frac{(1-x)^2(1+x)}{(1-x)^2 + x r_{\phi'}^2}, \\ C_{A'} &= \int_0^1 dx \frac{x(1-x)(2-x)r_{A'}^2 + x^3}{x^2 + (1-x)r_{A'}^2} \end{aligned} \tag{4}$$

and $r_{\phi'} \equiv m_{\phi'}/m_\mu$, $r_{A'} \equiv m_{A'}/m_\mu$. The contribution to $g_\mu - 2$ from ϕ' is always positive, while the contribution from A' is always negative, as the A' has both vector and axial couplings to the muon. These contributions must cancel to within $\mathcal{O}(1\%)$ in order for the total correction to $g_\mu - 2$ to be consistent with observations. We plot $C_{\phi'}(r_{\phi'})$ and $C_{A'}(r_{A'})$ in Fig. 2.

Interestingly, the contribution from the A' is nearly universal; $C_{A'}$ only varies between 1/2 and 2/3. In particular, as $m_{A'}$ grows, the coupling also grows and the contribution to $g_\mu - 2$ asymptotes to a constant. But even as $m_{A'}$ decreases and the gauge coupling goes to zero, the contribution to $g_\mu - 2$ still asymptotes to a constant, because the longitudinal polarization effectively becomes a pseudoscalar Goldstone mode, with the same coupling to muons as the ϕ'. As such, $g_\mu - 2$ can only be consistent with experiment for $C_{\phi'}$ between 1/2 and 2/3, which corresponds $(2/3)m_\mu \lesssim m_{\phi'} \lesssim m_\mu$. We thus see that one can only obtain consistency with $g_\mu - 2$ measurements for $m_{\phi'}$ within the very narrow range of ~67–100 MeV. Note that two-loop Barr-Zee type diagrams are also possible with dark Higgs/photon in this scenario. But the contribution is negligible compared to the one-loop contribution [57,58].

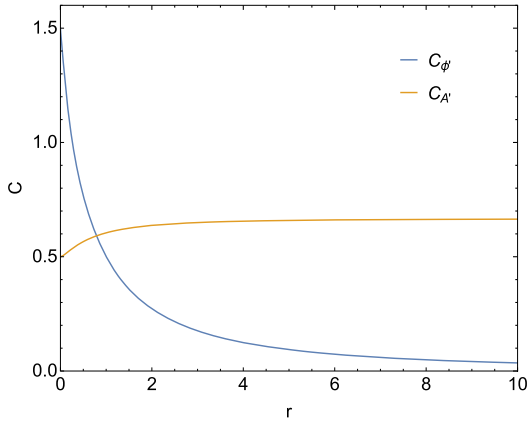

FIG. 2. Plot of $C_{\phi'}$ and $C_{A'}$ as functions of $r_{\phi'}$ and $r_{A'}$, respectively.

Thus far, we have only considered the low-energy effective field theory defined below the scale of electroweak symmetry breaking. But the muon mass term requires both a Higgs and a dark Higgs insertion, and thus arises from a nonrenormalizable operator of the form $(1/\Lambda)H\phi\bar{\mu}\mu$ in the theory defined above electroweak symmetry breaking. There should be some UV completion of this theory, and one might wonder if the corrections to $g_\mu - 2$ induced by the new UV fields could spoil the result we have found. To explore this, we consider, as an example of a possible UV completion, the universal seesaw [59–66]. In this case, there is a new heavy fermion χ_μ, charged under hypercharge, which couples to muons as $\lambda_L H\bar{\chi}_\mu P_L\mu + \lambda_R\phi\bar{\chi}_\mu P_R\mu + \text{H.c.}$. In the theory defined below m_{χ_μ}, this will yield the required effective operator, subject to the seesaw relation $m_\mu \sim \lambda_L\lambda_R\langle H\rangle V/m_{\chi_\mu}$. If we take $V = 10$ GeV and $\lambda_{L,R} = \mathcal{O}(1)$, then we find $m_{\chi_\mu} = \mathcal{O}(10\ \text{TeV})$; the corrections yielded by introducing this field will not substantially change our discussion. Note that if $\lambda_L\lambda_R$ is significantly smaller than unity, then χ_μ may be light enough to be probed at the LHC.

III. ALLOWED REGIONS OF PARAMETER SPACE AND FUTURE PROBES

We will now consider the regions of this parameter space are consistent with other laboratory experiments. The relevant experiments are those in which the A' and ϕ' are produced at accelerator experiments and either decay invisibly, or decay visibly at displaced detectors [10].

If the A' decays invisibly, then this scenario would be ruled out by data from COHERENT [67–71] and Crystal Barrel [72,73], unless $m_{A'} < 30$ MeV. But for $m_{A'} \lesssim \mathcal{O}(10\ \text{MeV})$, this scenario faces tension with cosmological bounds (corrections to N_{eff} [11,74]), although there are more complicated scenarios in which this tension

can be alleviated. For $m_{A'}$ in the ∼10–30 MeV range, A' production can potentially contribute to anomalous supernova cooling [75–78]). But in this mass range, the coupling g_{T3R} is large enough that the A' will decay promptly, and the decay products will not be able to free stream out of the supernova. If A' in the ∼10–30 MeV mass range decays invisibly, then it will satisfy all other current laboratory and cosmological constraints, and the constraints on $g_\mu - 2$ will also be satisfied for $m_{\phi'}$ in the ∼95–102 MeV range.

Moreover, for $m_{A'} \sim 30$ MeV, this scenario can explain the excess of events seen by the COHERENT experiment. The COHERENT experiment collides a proton beam against a fixed target, and searches for the scattering of neutrinos produced by these collisions at a displaced detector. The COHERENT experiment sees a $2.4 - 3\sigma$ excess of events [79], which could be explained if the A' ($m_{A'} \sim 30$ MeV) decays to either dark matter or sterile neutrinos, which in turn scatter against nuclei in the distant detector by A' exchange [10].

This scenario, in which the A' ($m_{A'} \in [10, 30]$ MeV) and ϕ' ($m_{\phi'} \in [95, 102]$ MeV) decay invisibly, can be probed definitively by the upcoming NA-64μ and LDMX-M^3 experiments. We will address the scenario of invisible A' decay further, in the context of flavor anomalies.

The visible decay $A' \to e^+e^-$ can be mediated by one-loop kinetic mixing, in which the right-handed SM fermions charged under $U(1)_{T3R}$ run in the loop. Assuming no tree-level kinetic mixing, we find a $\gamma - A'$ kinetic mixing parameter of $\epsilon \sim (m_{A'}/\sqrt{2}V)\sqrt{\alpha_{em}/4\pi^3}$. This scenario is ruled out by data from U70/NuCal unless $m_{A'} > 56$ MeV, and by data from *BABAR* [42,80,81] unless $m_{A'} < 200$ MeV. For $m_{A'}$ in the 56–200 MeV range, the range of $m_{\phi'}$ for which $g_\mu - 2$ can match observation is indeed very narrow: 74–86 MeV. We plot the region of $(m_{\phi'}, m_{A'})$ parameter space consistent with current $g_\mu - 2$ observations in Fig. 3, along with current bounds from U70/NuCal, *BABAR* and E137 [82–84]. We also plot the sensitivity of FASER, FASER 2, SHiP and SeaQuest, which also can search for the displaced decays of A'. These bounds and sensitivities are discussed in more detail in [10].

Note that, if we increase the value of V, then we will reduce the precision with which $C_{\phi'}$ and $C_{A'}$ must cancel. But increasing V will also result in a longer lifetime for A', since it would yield a reduced gauge coupling for $U(1)_{T3R}$. This would raise the lower bound on $m_{A'}$ from U70/NuCal, which is determined by fact that, for larger $m_{A'}$, the dark photon decays before it reaches the detector. Thus, one cannot significantly reduce the precision of the required cancellation by increasing V.

A. Dark matter relic density and direct detection

The motivation for coupling the light fermions to $U(1)_{T3R}$ was for the new light scale to not only feed into the light SM fermion masses but also the dark sector,

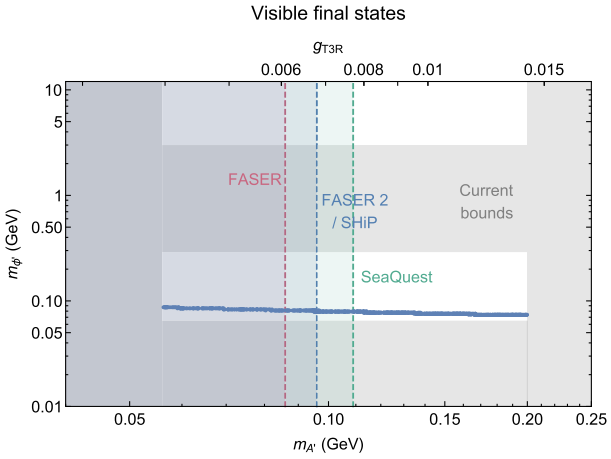

FIG. 3. Plot of the region in the $(m_{A'}, m_{\phi'})$ plane which is consistent with current measurements of $g_\mu - 2$ (blue), along with current exclusion bounds (gray) from U70/NuCal, E137 and *BABAR*, and the future sensitivity of FASER (red transparent), FASER 2/SHiP (blue transparent) and SeaQuest (green transparent). g_{T3R} is shown on the top axis.

providing a predictive framework for determining the dark matter mass scale. The dark sector consists of two Majorana fermions, $\eta_{1,2}$ which couple to ϕ' ($\propto m_\eta/V$) and A' ($\propto m_{A'}/V$) These couplings allow the dark particles to interact with the SM, potentially diluting the relic density, and yielding a direct detection signal.

Dark matter coannihilation in the early Universe can be mediated by the A', but the only accessible final states are $\nu_A\nu_A$ and e^+e^- (the $\gamma\gamma$ final state is forbidden by the Landau-Yang theorem [85]). Since both of these final states are suppressed, either by a neutrino mixing angle or a kinetic mixing parameter, coannihilation via an intermediate A' will play no role in our benchmark scenario.

For $m_\eta \sim (1/2)m_{\phi'}$, the relic density can instead be sufficiently depleted by annihilation to photons via the ϕ' resonance ($\eta\eta \to \phi' \to \gamma\gamma$) to match current observations. Note that this annihilation cross section is p-wave suppressed. This suppression was only an $\mathcal{O}(10)$ factor at the time of dark matter freeze-out, but was much larger at late times, leading to a negligible contribution to cosmic microwave background distortions or current indirect detection signatures.

Dark matter spin-independent velocity-independent scattering with nuclei can be mediated by either the ϕ' or A', which in this scenario couple both to the dark matter and to u/d quarks. Scattering mediated by ϕ' is elastic and isospin invariant, while scattering mediated by the A' is inelastic (since Majorana fermions can only have off-diagonal vector couplings) and maximally isospin violating [86–88] (since the A' couples to u and d with opposite signs).

In Fig. 4, we plot the elastic spin-independent dark matter nucleon scattering cross section mediated by ϕ', assuming $m_{\phi'} = 75$ MeV. In the same plot, we also show the inelastic spin-dependent dark matter proton scattering

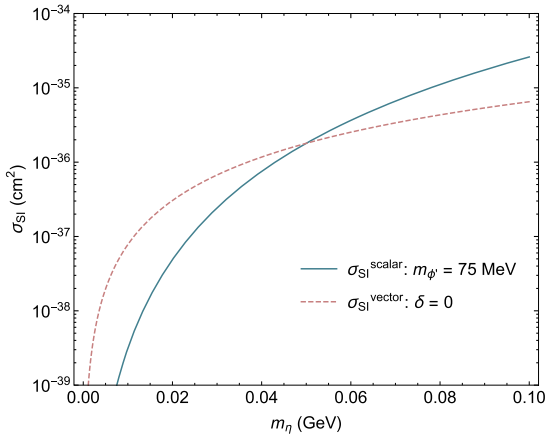

FIG. 4. Spin-independent dark matter-nucleon scattering cross section as a function of the dark matter mass. The blue (solid) line shows the spin-independent (SI) elastic scattering cross section mediated by ϕ' for $m_{\phi'} = 75$ MeV. And the orange (dashed) line shows the SI inelastic scattering cross section mediated by A' with $\delta = 0$.

cross section mediated by A', assuming that the dark matter mass splitting is negligible. Note that this cross section is independent of $m_{A'}$ at fixed V, since $g_{T3R} \propto m_{A'}$. For $m_{\eta_1} \lesssim 100$ MeV, these scenarios are unconstrained by current direct detection experiments [89–92].

IV. FLAVOR ANOMALIES

This model can potentially impact the variety of anomalies in observables based on the process $b \to s\ell^+\ell^-$. If these anomalies are explained by new physics, it points to a scenario which generates both lepton flavor nonuniversality and quark flavor violation. The scenario we describe here can contribute to both of the above, implying that it may also contribute to these flavor anomalies.

Lepton flavor nonuniversality arises from the low-energy sector of the theory, since the ϕ' and A' couple only to μ at tree level. On the other hand, quark flavor violation can arise from the UV completion of this model. We have considered, as possible UV completions, the addition of heavy fermions which have same EM charge as SM fermions but different charges under $SU(2)_L$ and/or $U(1)_{T3R}$. Once these heavy fermions are integrated out, we generate the low energy effective Lagrangian as described in the Appendix.

When these new fermions are added, the Z and A' couplings to fermions in the flavor eigenstate basis are diagonal matrices which need not be proportional to the identity. As a result, these coupling matrices can become nondiagonal in the mass eigenstate basis, yielding vertices of the form $\bar{b}\gamma^\mu P_{L,R} s(Z, A')_\mu$. Note, such flavor changing is not allowed for the photon coupling, as a result of gauge invariance (in particular, the photon coupling matrix is proportional to the identity in every basis). Terms of the form $\bar{b}\gamma^\mu P_{L,R} s Z_\mu$ can contribute to universal quark flavor-changing processes ($b \to s\ell^+\ell^-$), while terms of the form $\bar{b}\gamma^\mu P_{L,R} s A'_\mu$ can contribute to lepton nonuniversal quark flavor-changing processes ($b \to s\mu^+\mu^-$).

As an example, we have considered a UV completion based on the universal seesaw, in which one introduces new heavy vectorlike fermions $\chi_{u,d,\mu,\nu}$ which are neutral under $U(1)_{T3R}$, but have the same SM quantum numbers as u_R, d_R, μ_R and ν_R, respectively. While this is a minimal UV completion, one could add additional generations of these heavy particles, or even a single additional particle, without generating anomalies. Consider adding an additional χ'_a, which mixes with b and s through Lagrangian terms of form $\lambda'_{b,s} H \bar{Q}_L^{b,s} P_R \chi'_a + m'_{b,s} \bar{\chi}'_a P_R q_R^{b,s} + H.c.$. (we assume negligible mixing with the first generation). We see that $(\chi'_a)_R$ has same Z coupling as $(b, s)_R$, while $(\chi'_a)_L$ has a Z coupling which differs from $(b, s)_L$, and $(b, s, \chi'_a)_{L,R}$ are all neutral under $U(1)_{T3R}$. In this scenario, we would find a vertex of the form $\bar{b}\gamma^\mu P_L s Z_\mu$ at tree level [Fig. 5(a)], but with no similar coupling for right-handed quarks (since the Z coupling to the right-handed quarks is the identity in every basis). A coupling of the form $\bar{b}\gamma^\mu P_L s A'_\mu$ is also induced at one-loop through $Z - A'$ kinetic mixing, but this term will generally be small if the kinetic mixing is small.

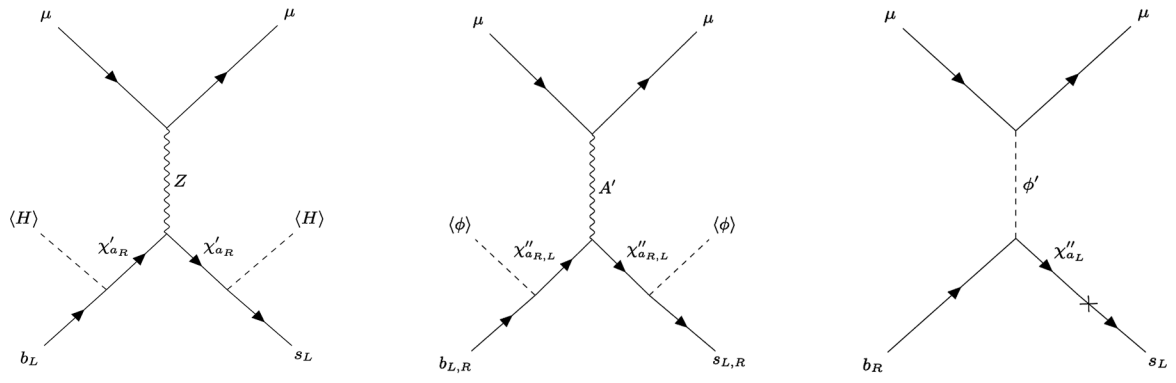

FIG. 5. Feynman diagrams that contribute to the B anomalies.

By the same token, one could instead add a vectorlike fermion χ''_a with the same SM quantum numbers as $(b,s)_R$ but with $U(1)_{T3R}$ charge $Q_{T3R}=2$. This fermion could mix with b, s (we assuming negligible mixing with d) through a Lagrangian term of the form $\lambda''_{b,s}\phi\bar{\chi}''_a P_R q_{b,s}$. Since χ''_a is charged under $U(1)_{T3R}$ while b, s are not, this term will yield a tree-level contribution to the coupling $\bar{b}\gamma^\mu P_{L,R} s A'_\mu$ [Fig. 5(b)]. Similarly, since $(\chi''_a)_L$ has a different Z coupling than $(b,s)_L$, this term will yield a tree-level contribution to the coupling $\bar{b}\gamma^\mu P_L s Z_\mu$. In this case, there is no similar contribution to $\bar{b}\gamma^\mu P_R s Z_\mu$, since $(b,s,\chi''_a)_R$ all have identical coupling to the Z boson. These considerations would be reversed if we had instead given the χ''_a the same SM gauge charges as $(b,s)_L$.

Note that the introduction of χ''_a will also induce a vertex of the form $\lambda''_{b,s}\phi'\bar{q}_{L(s,b)}q_{R(b,s)}\sin\theta'_{(s,b)L}$. The related diagram is shown in Fig. 5(c).

We can approximate the effect of these interactions with effective operators which couple a $(b,\ s)$ quark bilinear to a muon bilinear. For diagrams in which ϕ' or A' is exchanged, since the energy transfer is much larger than the mediator, we may approximate the energy scale of the operator with energy scale of the process, $\Lambda\sim\mathcal{O}(2\text{ GeV})$.

The diagrams which involve ϕ' exchange will contribute to effective operators with scalar Lorentz structure. The diagrams which involve Z or A' exchange will contribute to effective operators with vector or axial-vector Lorentz structure, and also to operators with pseudoscalar structure (arising from the Goldstone mode, or equivalently, the chiral coupling of the longitudinal polarization). We may ignore this operator for the case of Z exchange, however, since the mass of the gauge boson is much larger than the energy of the process.

The effective operator corresponding to Fig. 5(a) can be written as

$$\mathcal{O}^Z_U=\frac{e^2}{3m_Z^2}\tan^2\theta_W(\sin\theta_{sL}\sin\theta_{bL}+\sin\theta'_{sL}\sin\theta'_{bL})\times(\bar{b}\gamma^\mu P_L s)\left(\bar{\mu}\gamma_\mu\left[P_R+\left(1-\frac{1}{2\sin^2\theta_W}\right)P_L\right]\mu\right). \quad (5)$$

We can express the effective operators corresponding to Figs. 5(b) and 5(c) as

$$\mathcal{O}^{A'}_{NU}=\frac{1}{\Lambda^2}\sin\theta'_{s(L,R)}\sin\theta'_{b(L,R)}\left(\frac{m_{A'}}{\sqrt{2}V}\right)^2\times(\bar{b}\gamma^\mu P_{L,R}s)(\bar{\mu}\gamma_\mu P_R\mu)+\frac{1}{\Lambda^2}\sin\theta'_{s(R)}\sin\theta'_{b(R)}\left(\frac{m_\mu m_b}{2V^2}\right)(\bar{b}\gamma^5 s)(\bar{\mu}\gamma^5\mu)-\frac{1}{\Lambda^2}\sin\theta'_{s(L)}\sin\theta'_{b(L)}\left(\frac{m_\mu m_s}{2V^2}\right)(\bar{b}\gamma^5 s)(\bar{\mu}\gamma^5\mu), \quad (6)$$

$$\mathcal{O}^{\phi'}_{NU}=\frac{\lambda''_s}{\Lambda^2}\sin\theta'_{bL}\frac{m_\mu}{\sqrt{2}V}(\bar{b}P_R s)(\bar{\mu}\mu)+\frac{\lambda''_b}{\Lambda^2}\sin\theta'_{sL}\frac{m_\mu}{\sqrt{2}V}(\bar{b}P_L s)(\bar{\mu}\mu), \quad (7)$$

where $\theta_{(s,b)L}$ are the left-handed $(s,b)-\chi'_a$ mixing angles, $\theta'_{(s,b)(L,R)}$ are the left-/right-handed $(s,b)-\chi''_a$ mixing angles and where we may take $\Lambda\sim\mathcal{O}(2\text{ GeV})$.

We can expand these operators in the basis

$$\frac{\alpha_{em}G_F}{\sqrt{2}\pi}V_{tb}V^*_{ts}\sum_{i,\ell}C_i^{bs\ell\ell}\mathcal{O}_i^{bs\ell\ell}, \quad (8)$$

where

$$\begin{aligned}
\mathcal{O}_9^{bs\ell\ell}&=(\bar{s}\gamma^\mu P_L b)(\bar{\ell}\gamma_\mu\ell),\\
\mathcal{O}_{10}^{bs\ell\ell}&=(\bar{s}\gamma^\mu P_L b)(\bar{\ell}\gamma_\mu\gamma^5\ell),\\
\mathcal{O}'^{bs\ell\ell}_9&=(\bar{s}\gamma^\mu P_R b)(\bar{\ell}\gamma_\mu\ell),\\
\mathcal{O}'^{bs\ell\ell}_{10}&=(\bar{s}\gamma^\mu P_R b)(\bar{\ell}\gamma_\mu\gamma^5\ell),\\
\mathcal{O}_S^{bs\ell\ell}&=m_b(\bar{s}P_R b)(\bar{\ell}\ell),\\
\mathcal{O}'^{bs\ell\ell}_S&=m_b(\bar{s}P_L b)(\bar{\ell}\ell),\\
\mathcal{O}_P^{bs\ell\ell}&=m_b(\bar{s}P_R b)(\bar{\ell}\gamma^5\ell),\\
\mathcal{O}'^{bs\ell\ell}_P&=m_b(\bar{s}P_L b)(\bar{\ell}\gamma^5\ell).
\end{aligned} \quad (9)$$

Defining $C_i^U=C_i^{bsee}$ and $C_i^{NU}=C_i^{bs\mu\mu}-C_i^U$, we find

$$\begin{aligned}
\Delta C_9^U&=(-146)(\sin\theta_{sL}\sin\theta_{bL}+\sin\theta'_{sL}\sin\theta'_{bL}),\\
\Delta C_{10}^U&=(1.8\times10^3)(\sin\theta_{sL}\sin\theta_{bL}+\sin\theta'_{sL}\sin\theta'_{bL}),\\
\Delta C_9^{NU}&=\Delta C_{10}^{NU}=(1.9\times10^8)\sin\theta'_{sL}\sin\theta'_{bL}\left(\frac{m_{A'}}{\sqrt{2}V}\right)^2,\\
\Delta C_9'^{NU}&=\Delta C_{10}'^{NU}=(1.9\times10^8)\sin\theta'_{sR}\sin\theta'_{bR}\left(\frac{m_{A'}}{\sqrt{2}V}\right)^2,\\
\Delta C_P^{NU}&=-\Delta C_P'^{NU}=-(2.0\times10^5\text{ GeV}^{-1})\left(\frac{V}{10\text{ GeV}}\right)^{-2}\\
&\quad\times(\sin\theta'_{sR}\sin\theta'_{bR}-(m_s/m_b)\sin\theta'_{sL}\sin\theta'_{bL}),\\
\Delta C_S^{NU}&=(2.7\times10^7\text{ GeV}^{-1})\lambda''_b\sin\theta'_{sL}\frac{m_\mu}{m_b}\left(\frac{V}{10\text{ GeV}}\right)^{-1},\\
\Delta C_S'^{NU}&=(2.7\times10^7\text{ GeV}^{-1})\lambda''_s\sin\theta'_{bL}\frac{m_\mu}{m_b}\left(\frac{V}{10\text{ GeV}}\right)^{-1}.
\end{aligned} \quad (10)$$

Since $\sin^2\theta_W\sim0.23$, the universal lepton vector coupling is negligible.

We see that this scenario allows for several operators which contribute $b\to s\ell^+\ell^-$ processes, with coefficients controlled by independently tunable couplings and mixing angles. We find that we have freedom in the quark

couplings, although the vector couplings to muons are only right handed.

A. Benchmark scenarios

We now use the allowed parameter space of $m_{A'}$ and $m_{\phi'}$ masses, as shown in Fig. 3, to explain the recently observed anomalies. To study the implications of this scenario for flavor anomalies, we restrict our analysis to theoretically clean observables [93], R_K, R_{K^*} and $\mathrm{Br}(B_s \to \mu^+\mu^-)$. R_K and R_{K^*} are defined as

$$R_K \equiv \frac{\mathrm{Br}(B \to K\mu^+\mu^-)}{\mathrm{Br}(B \to Ke^+e^-)},$$
$$R_{K^*} \equiv \frac{\mathrm{Br}(B \to K^*\mu^+\mu^-)}{\mathrm{Br}(B \to K^*e^+e^-)}. \tag{11}$$

Because of lepton flavor universality, the SM predictions for R_K and R_{K^*} are close to unity [36,37], while the measurements have been consistently below the SM prediction [33–35,94,95]. Recently, the LHCb collaboration reported the most precise measurement of R_K in the q^2 bin of 1.1 to 6 GeV^2 using the full run-1 and run-2 datasets shown in Eq. (2) [35], which deviates form the SM prediction by 3.1σ. The R_{K^*} measurements [33,34]

$$R_{K^*} = \begin{cases} 0.660^{+0.11}_{-0.07} \pm 0.03 & (2m_\mu)^2 < q^2 < 1.1\ \mathrm{GeV}^2 \\ 0.685^{+0.11}_{-0.07} \pm 0.051 & 1.1\ \mathrm{GeV}^2 < q^2 < 6\ \mathrm{GeV}^2 \end{cases} \tag{12}$$

disagree with the SM expectations at the 2.4σ and 2.5σ levels, respectively. In this study, we restrict ourselves to the central bin of R_{K^*} measurement. It is known that explaining both bins with effective operators is extremely challenging, and we will wait for more data to confirm the energy dependency [96,97]. Together with other processes mediated by $b \to s\ell^+\ell^-$ transitions, the tension is at least at the level of 4σ [93,98,99]. LHCb also reported the measurement of the branching fraction of $B_s \to \mu^+\mu^-$ using the full dataset [100],

$$\mathrm{Br}(B_s \to \mu^+\mu^-) = 3.09^{+0.46}_{-0.43}(\mathrm{stat})^{+0.15}_{-0.11}(\mathrm{sys}) \times 10^{-9}. \tag{13}$$

Together with the recent measurement by ATLAS [101] and CMS [102], a decay rate smaller than the SM prediction is favored [93,98].

In general, it is difficult to explain $g_\mu - 2$, $R_{K^{(*)}}$, and $B_s \to \mu^+\mu^-$ simultaneously with a vector mediator while respecting all current experimental constraints. The region that is consistent with $g_\mu - 2$ is strongly constrained by beam dump and fixed target experiments for models such as $U(1)_{B-L}$ [42]. In models such as $U(1)_{L_\mu - L_\tau}$ [103,104], a mediator around 10–100 MeV with a coupling $g_{\mu\tau} \sim \mathcal{O}(10^{-4})$–$\mathcal{O}(10^{-3})$ can accommodate the $g_\mu - 2$ results. Heavier mediators require larger muon couplings and are heavily constrained by neutrino trident production at CCFR [42]. Then to accommodate the result of R_K and R_{K^*}, a bs coupling around $\mathcal{O}(10^{-10})$–$\mathcal{O}(10^{-9})$ is required. In this scenario, a light mediator decays dominantly to neutrinos, and it contributes to the $B \to K^*X, X \to \nu\nu$ process. The couplings required to explain $R_{K^{(*)}}$ lead to $\mathrm{Br}(B \to K^*X) \times \mathrm{Br}(X \to \nu\nu)$ at least $\mathcal{O}(10^{-4})$. The measurement at Belle sets an upper limit on $\mathrm{Br}(B \to K^*\nu\nu)$ of 5.5×10^{-5} at 90% confident level [105], and thus exclude this simple scenario.

The advantage of models with only right-handed lepton coupling such as $U(1)_{T3R}$ is that, due to the lack of left-handed neutrino couplings, the major experimental constraints, including CCFR and $B \to K^*\nu\nu$, do not apply to such scenarios.[1] But on the other hand, $U(1)_{T3R}$ models necessarily impose $C_9^{(\prime)NU} = C_{10}^{(\prime)NU}$, and this constraint makes it difficult to explain the R_K and R_{K^*}, and $\mathrm{Br}(B_S \to \mu^+\mu^-)$ measurements simultaneously. The R_K and R_{K^*} measurements prefers a negative $C_9^{bs\mu\mu}$, or a positive $C_{10}^{bs\mu\mu}$, and the smaller decay rate of $B_s \to \mu^+\mu^-$ favors a positive $C_{10}^{bs\mu\mu}$, or a negative $C_{10}^{\prime bs\mu\mu}$. To explain R_K and R_{K^*} with a positive $C_{10}^{bs\mu\mu}$, which is favored by $B_s \to \mu^+\mu^-$, implies a negative $C_9^{bs\mu\mu}$. Since $C_9^{NU} = C_{10}^{NU}$, a negative $C_9^{bs\mu\mu}$ and a positive $C_{10}^{bs\mu\mu}$ imply a negative nonuniversal part and a positive universal part. Then a positive C_{10}^{bsee} will leave the R_K and R_K^* unexplained.

Therefore, we consider the following two additional scenarios. In the first scenario, we introduce scalar and pseudoscalar couplings. We rely on the scalar and pseudoscalar operators to explain $\mathrm{Br}(B_S \to \mu^+\mu^-)$, while $R_{K^{(*)}}$ can be fixed by other operators. In the second scenario, we include the prime operators, which only contain the nonuniversal part, so that the contributions are generated from both left-handed and right-handed quark couplings.

In Table I, we present four benchmarks. For all benchmark points, we calculate the corresponding flavor observables with FLAVIO [110], and also calculate the SM pull, defined as $\sqrt{\Delta\chi^2}$, using the clean observables only, to show how well those three measurements can be described and how significant the deviation is from the SM. When we calculate the SM pull, we only include the LHCb results for simplicity. The Belle measurements of $R_{K^{(*)}}$ have

[1] In this scenario, there is a contribution to the $B \to K^{(*)}\nu\nu$ process from $B \to K^{(*)}A'$, and $A' \to \nu\nu$. These processes have hadronic form factor uncertainties [106–108]. In addition, in the Belle and *BABAR* analysis [105,109], the invariant mass of the two neutrinos, $m_{\nu\nu}$ is required to be larger than about 2.5 GeV. Therefore, such measurements do not apply to the parameter space if A' dominantly decays into missing energy, i.e., $\nu_s\nu_s$. There would be constraints from the COHERENT and Crystal Barrel experiments for such a final state in this model for $m_{A'} > 30$ MeV. However for $m_{A'} < 30$ MeV all constraints are satisfied.

TABLE I. Details of the four benchmark points described in the text. The first five rows present the values of the coefficients C_{10}^U, $C_{9,10}^{NU}$, $|C_s - C_s'|$ (in units of GeV^{-1}), $|C_p - C_p'|$ (in units of GeV^{-1}), and $C_{9,10}'^{NU}$. Rows 6–8 present predictions for R_K, R_{K^*} (in the $q^2 \in [1.1, 6]$ GeV^2 bin), and $\mathrm{Br}(B_s \to \mu^+\mu^-)$. Row 9 presents the SM pull of each benchmark point.

	BMA	BMB	BMC	BMD
C_{10}^U	4.85	−5.86	2.7	−5.67
$C_{9,10}^{NU}$	−0.30	3.65	−0.8	4.55
$\lvert C_s - C_s'\rvert$ GeV^{-1}	0.033	0.024	0.011	…
$\lvert C_p - C_p'\rvert$ GeV^{-1}	…	0.030	0.043	…
$C_{9,10}'^{NU}$	…	…	…	−1.28
R_K	0.82	0.87	0.86	0.87
$R_K^*[1.1, 6]$	0.83	0.78	0.97	0.89
$\mathrm{Br}(B_s \to \mu^+\mu^-)$	3.36×10^{-9}	3.05×10^{-9}	2.67×10^{-9}	3.34×10^{-9}
SM pull	4.4σ	4.6σ	3.8σ	4.2σ

significantly larger uncertainties compared to the LHCb results [33–35], while the $B_s \to \mu^+\mu^-$ measurements by ATLAS and CMS correlates with $B_d \to \mu^+\mu^-$ [101,102]. The energy-dependant behavior in R_{K^*} is beyond the scope of this study, so we only list the value of R_{K^*} in the central q^2 bin, as indicated by numbers in the bracket. Here q^2 is defined as the invariant mass squared of the dimuon system.

The first three benchmarks correspond to the first scenario in which scalar and pseudoscalar operators are responsible for $\mathrm{Br}(B_S \to \mu^+\mu^-)$. In BMA, we include the scalar operators, and in BMB, and in BMC, we include both scalar and pseudoscalar operators. For BMA, R_K and $B_s \to \mu^+\mu^-$ agree with the LHCb results within 1σ, and R_{K^*} agree with the LHCb results within 2σ, and the SM pull is 4.4σ for BMA. For the second benchmark BMB, all three observables agree with the LHCb measurements within 1σ, with a SM pull of 4.6σ. For BMC, R_K and $B_s \to \mu^+\mu^-$ agree with the LHCb results within 1σ, while R_{K^*} is SM like.

BMD corresponds to the second scenario. Introducing only left-handed quark couplings does not provide a good explanation for all three measurements. As discussed above, a pure left-handed quark coupling will leave either R_{K^*} or $\mathrm{Br}(B_s \to \mu^+\mu^-)$ unexplained. Therefore, we further include the nonuniversal, primed operators. R_K and $B_s \to \mu^+\mu^-$ agree with the LHCb results within 1σ, and R_{K^*} agree with the LHCb results within 2σ, and the SM pull is 4.7σ for BMD.

In BMA and BMC, with a negative C_9 and a positive C_{10}, both electron and muon modes are suppressed compared to the SM, and R_K and R_{K^*} are explained by suppressing the muon mode even more from the nonuniversal part. In BMB and BMD, both electron and muon modes are enhanced compared to the SM, and R_K and R_{K^*} are explained by increasing the muon mode less from the nonuniversal part. For all benchmark scenarios we considered, the Z-mediated contributions to $B \to K^{(*)}\nu\nu$, and $B \to K^{(*)}ee$ are well below the current upper limit [105,111,112], and contributions to $B_s - \overline{B_s}$ mixing are negligible as $bsbs$ operators are very small in the region of interest.

We have listed in Table II the predictions of this model for other observables with large theoretical uncertainties. We also list the current experimental value and the SM predictions, calculated by FLAVIO [110] for references. Currently, those observables are measured with 3 fb^{-1} of data. The numbers in the bracket show the range of the invariant mass-squared of the dimuon system, q^2. The uncertainties in the experimental value, from left to right, are statistical, systematic and due to the normalisation mode (for the last two only). As discussed above, in BMA and BMC, the muon modes are suppressed, as indicated by the current experiments, while in BMB and BMD, the muon modes are enhanced compared to the SM.

Because of the universal contribution, in order to accommodate the experimental value of R_K and R_{K^*}, sizable deviations from SM predictions are expected for the unclean observables. Models with smaller Wilson coefficients, such as in BMB, lead to a good explanation to the unclean observables. These observables, however, involve form factor related uncertainties, which lead to large corrections to the model predictions. If these theoretical uncertainties can be brought under control, then model predictions can be more meaningfully compared to data.

Below the dimuon threshold, A' may decay to e^+e^- via kinetic mixing with the photon. In processes such as $B \to Ke^+e^-$ (which contain hadronic form factor uncertainties [106–108]), an A' can be produced on shell via $B \to KA'$, with the A' decaying to an e^+e^- pair, potentially leading to a signal in a resonance search. Although LHCb does have constraints on the dark photon using $\ell\ell$ resonance searches, it has no constraints on the e^+e^- decay mode in the energy range of interest. LHCb constraints use the $\mu^+\mu^-$ final state for $m_{A'} \geq 2m_\mu$ [116]. For $B \to K^*\ell\ell$

TABLE II. Predictions for observables for the four benchmark points described in the text (columns 4–7), along with the Standard Model prediction (third column) and the measured value with uncertainties (second column). The uncertainties, from left to right, are statistical, systematic and due to the normalization mode (for the last two only). Rows 1–3 consider $\mathrm{Br}(B^+ \to K^{*+}\mu^+\mu^-)(q^2 \in [15, 19]\ \mathrm{GeV}^2)$, $\mathrm{Br}(B^0 \to K^0\mu^+\mu^-)(q^2 \in [15, 19]\ \mathrm{GeV}^2)$ and $\mathrm{Br}(B^+ \to K^+\mu^+\mu^-)(q^2 \in [15, 22]\ \mathrm{GeV}^2)$, respectively, all in units of 10^{-8}. Row 4 considers $d\mathrm{Br}(B_S \to \phi\mu^+\mu^-)/dq^2$, in units of $10^{-8}\ \mathrm{GeV}^{-2}$, averaged over $q^2 \in [1, 6]\ \mathrm{GeV}^2$, while row 5 considers $d\mathrm{Br}(\Lambda_b^0 \to \Lambda\mu^+\mu^-)/dq^2$, in units of $10^{-7}\ \mathrm{GeV}^{-2}$, averaged over $q^2 \in [15, 20]\ \mathrm{GeV}^2$.

Observable	Measured value	SM	BMA	BMB	BMC	BMD
$\mathrm{Br}(B^+ \to K^{*+}\mu^+\mu^-)(10^{-8})[15.0, 19.0]$	$15.8^{+3.2}_{-2.9} \pm 1.1$ [113]	26.8 ± 3.6	7.80	82.9	10.4	92.4
$\mathrm{Br}(B^0 \to K^0\mu^+\mu^-)(10^{-8})[15.0, 22.0]$	$6.7 \pm 1.1 \pm 0.4$ [113]	9.8 ± 1.0	3.31	30.4	4.15	29.4
$\mathrm{Br}(B^+ \to K^+\mu^+\mu^-)(10^{-8})[15.0, 22.0]$	$8.5 \pm 0.3 \pm 0.4$ [113]	10.7 ± 1.2	3.59	33.0	4.5	32.0
$\frac{dB(B_S \to \phi\mu^+\mu^-)}{dq^2}(10^{-8}\ \mathrm{GeV}^{-2})[1.0, 6.0]$	$2.57^{+0.33}_{-0.31} \pm 0.08 \pm 0.19$ [114]	4.81 ± 0.56	1.60	16.8	2.28	18.7
$\frac{dB(\Lambda_b^0 \to \Lambda\mu^+\mu^-)}{dq^2}(10^{-7}\ \mathrm{GeV}^{-2})[15, 20]$	$1.18^{+0.09}_{-0.08} \pm 0.03 \pm 0.27$ [115]	0.71 ± 0.08	2.19	2.28	0.29	2.48

modes [117,118], LHCb performs a resonance (e^+e^-) analysis only for $q^2 > 6\ \mathrm{GeV}^2$, using the $J/\psi \to e^+e^-$ channel. Below $6\ \mathrm{GeV}^2$, there exists no resonance study providing the distribution $m_{\ell\ell}(q^2)$. The minimum angular separation between e^+ and e^- is also not given (e^+e^- is quite collimated for such a low A' mass, as in our scenario). LHCb also performs nonresonance studies of the invariant masses $m(K\pi\ell\ell)$ and $m(K\ell\ell)$ for the $B \to K^*\ell\ell$ and $B \to K\ell\ell$ decay modes, respectively which does not constrain our model. Since we consider $m_{A'} \sim 100$ MeV, one needs a dedicated resonance study with the e^+e^- final state to obtain constraints. Currently we do not have any constraint from LHCb on this resonance channel.

In this setup, we introduced mixing in the second and third generation down-type quark sector via heavy quarks, and we have discussed the associated predictions for flavor-changing neutral currents. But this scenario does not generate contributions to the Cabibbo-Kobayashi-Maskawa matrix. To do so, we would need to turn on mixing among all the generations of up- and down-type quarks [59–66].

V. CONCLUSION

Scenarios in which first-/second-generation right-handed SM fermions are charged under $U(1)_{T3R}$ are particularly interesting. Among all scenarios involving new gauge groups, this scenario is distinctive because the coupling of the new particles to the SM is constrained from below; because the new symmetry protects fermion masses, the coupling of the symmetry-breaking field to SM fermions is proportional to the fermion mass. This yields an attractive scenario in which the symmetry-breaking naturally sets not only the light SM fermion masses but also the mass scale of the dark sector, naturally pointing to sub-GeV dark matter. But the other side of this coin is that the symmetry-breaking field necessarily has a large coupling to SM fields, as it is proportional to the ratio of SM fermion mass and the symmetry-breaking scale, which is presumed to be not large. This coupling is inherited by the dark Higgs and the Goldstone mode (which is absorbed into the dark photon longitudinal polarization). This scenario thus faces tight constraints from searches for these mediators, and only a narrow range of parameter space is still viable.

These couplings are particularly relevant to the corrections to $g_\mu - 2$, as both the dark Higgs and dark photon yield corrections which are roughly two orders of magnitude too large. But within the small region of parameter space which is allowed by other experiments, the corrections from the dark photon and the dark Higgs can cancel, yielding an overall contribution which matches the latest measurements from Fermilab.

This scenario necessarily leads to lepton flavor nonuniversality arising from low-energy physics. Moreover, UV completions of this scenario can easily accommodate quark flavor violation. These are the required ingredients for explaining the anomalies in $R_{K^{(*)}}$ observation. We show that we can have necessary operators to explain the anomalies after satisfying $B_s \to \mu^+\mu^-$ constraint in the allowed parameter space where the $g_\mu - 2$ anomaly is also explained. In general, it is not easy to explain both anomalies after satisfying various constraints. Various neutrino related measurements restrict the parameter space of the models which utilize left handed muons to solve the $R_{K^{(*)}}$ puzzle. However, this problem is ameliorated in the context of the $U(1)_{T3R}$ model due to the absence of the left-handed neutrino couplings of A'. We also list predictions for a few more observables which can be tested in the future. The future measurements of $R_{K^{(*)}}$ would be crucial to probe this scenario. In addition, as an example, we show a possible UV completion of this scenario based on the universal seesaw mechanism. The new heavy vectorlike fermions introduced can lead to strong first-order electroweak phase transitions and the corresponding gravitational wave signal provides an additional probe to this scenario [119]. As a future work, the cosmological dynamics behind this scenario will be studied in further detail.

It is interesting to probe the allowed parameter space of this model with future experiments. Future searches at

experiments such as FASER, SeaQuest and SHiP may find evidence for the displaced decays of $A' \to e^+e^-$. But the difficulty is that the very fact that the dark photon and dark Higgs contributions to $g_\mu - 2$ must be canceled against each other shows that they were both large, leading to an A' decay rate which is larger than usually expected. As a result, the A' often decays before it reaches a displaced detector. To test this scenario definitively, it would be best to have an experiment with a shorter distance from the target to the displaced detector.

We can consider the properties needed by a future displaced detector experiment to probe these models. If $N_{A'}$ is the number of A' at characteristic energy E produced by the beam which would reach the detector if A' were stable, the number which reaches the detector at distance d away is $N_{A'} \exp[-d/d_{\rm dec}]$, where $d_{\rm dec}$ is the decay length for an A' of energy $E_{A'}$. If $d_{\rm decay} \ll d$, then most A' which reach the detector will decay shortly after. So if we set this number to be of order unity, as a rough estimate of the number of A' reaching the detector necessary for a signal to be detected above negligible background, then we find $d_{\rm dec} = d/\ln(N_{A'})$. $d_{\rm dec}$ is determined by the model, but $d/\ln(N_{A'})$ is entirely determined by the properties of the instrument, and is a function of the maximum typically energy of the produced A'. We plot this quantity as a function of $E_{A'}$ in Fig. 6.

An alternative would be to search for visible decays of the ϕ' ($\phi' \to \gamma\gamma$). Searches for this decay channel require a detailed study of ϕ' production mechanisms. It would be interesting to perform a more detailed study of the sensitivity of displaced decay experiments. Alternatively, one could search for the central production of ϕ' at the LHC; where it could appear either as missing energy, or as a monophoton or diphoton signal. It maybe possible to search for these signals in events where ϕ' receives a large transverse boost against a recoiling photon or jet. It would be interesting to study this possibility in greater detail.

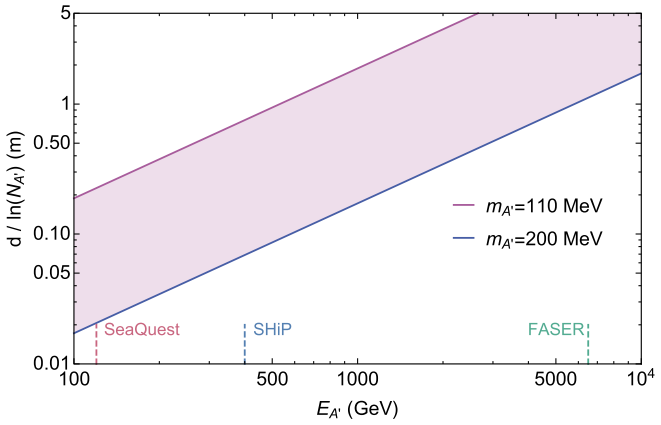

FIG. 6. A rough estimate of maximum $d/\ln(N_{A'})$ necessary for an experiment to be able to probe this scenario for $m_{A'} \in [110\ \text{MeV}, 200\ \text{MeV}]$, as a function of the maximum A' energy produced by the experiment. d is the displacement of the detector from the beam dump, and $N_{A'}$ is the number of A' at energy $E_{A'}$ produced in a beam aimed at the detector. The maximum A' energies of FASER, SHiP and SeaQuest are also shown.

ACKNOWLEDGMENTS

We would like to thank L. Darme and W. Parker for helpful discussions. The work of B. D. and S. G. are supported in part by the DOE Grant No. DE-SC0010813. The work of J. K. is supported in part by DOE Grant No. DE-SC0010504. The work of P. H. is supported by University of Nebraska-Lincoln, and National Science Foundation under Grant No. PHY-1820891. We have used the package TikZ-Feynman [120] to generate the Feynman diagram of Figs. 1 and 5.

APPENDIX: MODEL DESCRIPTION

The gauge symmetry of our model is $SU(3)_C \times SU(2)_L \times U(1)_Y \times U(1)_{T3R}$. The electric charge is defined as $Q = T3L + Y$, such that the new gauge group $U(1)_{T3R}$ is not connected to electric charge.

In addition to the light fields ϕ, A', η and ν_R (discussed in detail in the text and Ref. [9]), we add a set of heavy fermions $\chi_{u,d,\mu,\nu}$ which are singlets under $SU(2)_L$ and $U(1)_{T3R}$, and have same quantum numbers under $SU(3)_C$ and $U(1)_Y$ as u, d, μ and ν, respectively. These fermions will mix with the fermions charged under $U(1)_{T3R}$, generating the mass terms and couplings of the light fermions through a high-scale seesaw mechanism. The charge assignment of relevant particles are given in Table III.

The scalar potential can be written as

$$V = m_H^2 H^\dagger H + m_\phi^2 \phi^* \phi + \lambda_H (H^\dagger H)^2 + \lambda_\phi (\phi^* \phi)^2 + \lambda (H^\dagger H)(\phi^* \phi). \tag{A1}$$

Both scalar fields will get vevs, $\langle H \rangle = v/\sqrt{2}$ and $\langle \phi \rangle = V$. After the spontaneous symmetry breaking, the scalar fields can be written as

$$H = \begin{pmatrix} G^+ \\ \frac{1}{\sqrt{2}}(v + \rho_0 + iG_0) \end{pmatrix},$$
$$\phi = V + \frac{1}{\sqrt{2}}(\rho_\phi + iG_{\phi 0}). \tag{A2}$$

There are total 6 scalar degrees of freedom, out of which 4 are absorbed into the longitudinal polarizations of the $W^\pm, Z$ and A' gauge bosons. The remaining 2 are the physical Higgs and dark Higgs scalars. The CP-even states ρ_0 and ρ_ϕ mix and give rise to the two physical neutral scalar h and ϕ' with masses m_h and m'_ϕ, respectively. We identify h as the SM Higgs boson. The two physical neutral scalars in terms of the interaction states are given as

TABLE III. The charges of the fields under the gauge groups of the model. For the fermionic fields, the shown charges are for the left-handed component of each Weyl spinor.

Particle	$SU(3)_C \times SU(2)_L \times U(1)_Y \times U(1)_{T3R}$
χ_{uL}	$(3,1,2/3,0)$
χ_{dL}	$(3,1,-1/3,0)$
$\chi_{\mu L}$	$(1,1,-1,0)$
$\chi_{\nu L}$	(1,1,0,0)
χ^c_{uR}	$(3,1,-2/3,0)$
χ^c_{dR}	$(3,1,1/3,0)$
$\chi^c_{\mu R}$	(1,1,1,0)
$\chi^c_{\nu R}$	(1,1,0,0)
q_L	$(3,2,1/6,0)$
u^c_R	$(3,1,-2/3,-2)$
d^c_R	$(3,1,1/3,2)$
l_L	$(1,2,-1/2,0)$
μ^c_R	(1,1,1,2)
ν^c_R	$(1,1,0,-2)$
η_L	(1,1,0,1)
η^c_R	$(1,1,0,-1)$
H	$(1,2,1/2,0)$
ϕ	(1,1,0,2)

$$\begin{pmatrix} h \\ \phi' \end{pmatrix} = \begin{pmatrix} \cos\alpha & -\sin\alpha \\ \sin\alpha & \cos\alpha \end{pmatrix} \begin{pmatrix} \rho_0 \\ \rho_\phi \end{pmatrix}, \tag{A3}$$

where α is the mixing angle.

The decay rate for $h \to \phi'\phi'$ is constrained by LHC data. To remain consistent with this data, one must assume that λ (equivalently, α) is small.

The renormalizable Yukawa sector Lagrangian of the UV-complete model in the interaction basis is given by

$$\begin{aligned} -\mathcal{L}_Y = {} & \lambda_{Lu}\bar{q}'_L\chi'_{uR}\widetilde{H} + \lambda_{Ld}\bar{q}'_L\chi'_{dR}H \\ & + \lambda_{L\nu}\bar{l}'_L\chi'_{\nu R}\widetilde{H} + \lambda_{Ll}\bar{l}'_L\chi'_{\mu R}H + \lambda_{Ru}\bar{\chi}'_{uL}u'_R\phi^* \\ & + \lambda_{Rd}\bar{\chi}'_{dL}d'_R\phi + \lambda_{R\nu}\bar{\chi}'_{\nu L}\nu'_R\phi^* + \lambda_{Rl}\bar{\chi}'_{\mu L}\mu'_R\phi \\ & + m_{\chi_u}\bar{\chi}'_{uL}\chi_{uR} + m_{\chi_d}\bar{\chi}'_{dL}\chi_{dR} + m_{\chi_\nu}\bar{\chi}'_{\nu L}\chi_{\nu R} \\ & + m_{\chi_\mu}\bar{\chi}'_{\mu L}\chi_{\mu R} + m_D\overline{\eta}_R\eta_L + \frac{1}{2}\lambda_{\eta L}\overline{\eta}^c_L\eta_L\phi \\ & + \frac{1}{2}\lambda_{\eta R}\overline{\eta}^c_R\eta_R\phi^* + \text{H.c.}. \end{aligned} \tag{A4}$$

The fermionic flavor eigenstates will mix and give rise to the mass eigenstates. The mass matrix in the flavor eigenstate basis is given by

$$M_f = \begin{pmatrix} 0 & \frac{\lambda_{Lf}v}{\sqrt{2}} \\ \lambda_{Rf}V & m_{\chi'_f} \end{pmatrix}. \tag{A5}$$

The diagonalization of the fermionic mass matrix using the seesaw mechanism gives two mass eigenstates. The lightest mass eigenstates is the SM fermion while the heavier one is the physical vector-like fermion. The mass term for the SM fermion is

$$m_f = \frac{\lambda_{Lf}\lambda_{Rf}vV}{\sqrt{2}m_{\chi'_f}}, \tag{A6}$$

and the physical vectorlike fermion mass is

$$m_{\chi_f} \simeq m_{\chi'_f}. \tag{A7}$$

The neutrino mass matrix will be a more complicated 3×3 matrix since they can also get Majorana masses as both ν'_R and χ'_ν are uncharged under the unbroken SM gauge groups. The fermion mass eigenstates can be written in terms of the flavor eigenstates as follows:

$$\begin{pmatrix} f_{L,R} \\ \chi_{f_{L,R}} \end{pmatrix} = \begin{pmatrix} \cos\theta_{f_{L,R}} & \sin\theta_{f_{L,R}} \\ -\sin\theta_{f_{L,R}} & \cos\theta_{f_{L,R}} \end{pmatrix} \begin{pmatrix} f'_{L,R} \\ \chi_{f'_{L,R}} \end{pmatrix}, \tag{A8}$$

where $\theta_{f_{L,R}}$ are the mixing angles. In the high-scale seesaw limit, $m_{\chi_f} \gg \lambda_{Lf}v/2$, we get

$$\theta_{f_L} \simeq \tan^{-1}\left[\frac{\lambda_{Lf}v}{\sqrt{2}m_{\chi_f}}\right], \tag{A9}$$

and if $m_{\chi_f} \gg \lambda_{Rf}V$, then

$$\theta_{f_R} \simeq \tan^{-1}\left[\frac{\lambda_{Rf}V}{m_{\chi_f}}\right]. \tag{A10}$$

The mass matrix of the η field contains both Dirac terms, m_D, and Majorana terms, m_M. The Majorana term, m_M, is proportional to the vev V as $m_M = \lambda_M V$, where we assume that $\lambda_M = \lambda_{\eta L} = \lambda_{\eta R}$. We further assume that $m_M \gg m_D$. We get two Majorana fermions, η_1 and η_2, with masses $m_1 = m_M - m_D$ and $m_2 = m_M + m_D$, respectively.

In the low-energy effective field theory defined below the electroweak symmetry breaking scale, the interactions of the SM fermions and the dark matter fields, η, with the ϕ' is given by

$$\begin{aligned} -\mathcal{L} = {} & \frac{m_f}{\sqrt{2}V}\bar{f}f\phi' + \frac{m_1}{2\sqrt{2}V}\bar{\eta}_1\eta_1\phi' \\ & + \frac{m_2}{2\sqrt{2}V}\bar{\eta}_2\eta_2\phi'. \end{aligned} \tag{A11}$$

[1] G. W. Bennett *et al.* (Muon g-2 Collaboration), Phys. Rev. D **73**, 072003 (2006).
[2] M. Tanabashi *et al.* (Particle Data Group), Phys. Rev. D **98**, 030001 (2018).
[3] M. Davier, A. Hoecker, B. Malaescu, and Z. Zhang, Eur. Phys. J. C **80**, 241 (2020); **80**, 410(E) (2020).
[4] M. Davier, A. Hoecker, B. Malaescu, and Z. Zhang, Eur. Phys. J. C **77**, 827 (2017).
[5] T. Blum, P. A. Boyle, V. Gülpers, T. Izubuchi, L. Jin, C. Jung, A. Jüttner, C. Lehner, A. Portelli, and J. T. Tsang (RBCUKQCD Collaborations), Phys. Rev. Lett. **121**, 022003 (2018).
[6] A. Keshavarzi, D. Nomura, and T. Teubner, Phys. Rev. D **97**, 114025 (2018).
[7] T. Blum, N. Christ, M. Hayakawa, T. Izubuchi, L. Jin, C. Jung, and C. Lehner, Phys. Rev. Lett. **124**, 132002 (2020).
[8] F. Campanario, H. Czyż, J. Gluza, T. Jeliński, G. Rodrigo, S. Tracz, and D. Zhuridov, Phys. Rev. D **100**, 076004 (2019).
[9] B. Dutta, S. Ghosh, and J. Kumar, Phys. Rev. D **100**, 075028 (2019).
[10] B. Dutta, S. Ghosh, and J. Kumar, Phys. Rev. D **102**, 075041 (2020).
[11] B. Dutta, S. Ghosh, and J. Kumar, Phys. Rev. D **102**, 015013 (2020).
[12] B. Abi *et al.* (Muon g-2 Collaboration), Phys. Rev. Lett. **126**, 141801 (2021).
[13] T. Aoyama, M. Hayakawa, T. Kinoshita, and M. Nio, Phys. Rev. Lett. **109**, 111808 (2012).
[14] T. Aoyama, T. Kinoshita, and M. Nio, Atoms **7**, 28 (2019).
[15] A. Czarnecki, W. J. Marciano, and A. Vainshtein, Phys. Rev. D **67**, 073006 (2003); **73**, 119901(E) (2006).
[16] C. Gnendiger, D. Stöckinger, and H. Stöckinger-Kim, Phys. Rev. D **88**, 053005 (2013).
[17] G. Colangelo, M. Hoferichter, and P. Stoffer, J. High Energy Phys. 02 (2019) 006.
[18] M. Hoferichter, B.-L. Hoid, and B. Kubis, J. High Energy Phys. 08 (2019) 137.
[19] A. Keshavarzi, D. Nomura, and T. Teubner, Phys. Rev. D **101**, 014029 (2020).
[20] A. Kurz, T. Liu, P. Marquard, and M. Steinhauser, Phys. Lett. B **734**, 144 (2014).
[21] K. Melnikov and A. Vainshtein, Phys. Rev. D **70**, 113006 (2004).
[22] P. Masjuan and P. Sánchez-Puertas, Phys. Rev. D **95**, 054026 (2017).
[23] G. Colangelo, M. Hoferichter, M. Procura, and P. Stoffer, J. High Energy Phys. 04 (2017) 161.
[24] M. Hoferichter, B.-L. Hoid, B. Kubis, S. Leupold, and S. P. Schneider, J. High Energy Phys. 10 (2018) 141.
[25] A. Gérardin, H. B. Meyer, and A. Nyffeler, Phys. Rev. D **100**, 034520 (2019).
[26] J. Bijnens, N. Hermansson-Truedsson, and A. Rodríguez-Sánchez, Phys. Lett. B **798**, 134994 (2019).
[27] G. Colangelo, F. Hagelstein, M. Hoferichter, L. Laub, and P. Stoffer, J. High Energy Phys. 03 (2020) 101.
[28] G. Colangelo, M. Hoferichter, A. Nyffeler, M. Passera, and P. Stoffer, Phys. Lett. B **735**, 90 (2014).
[29] S. Borsanyi *et al.*, Nature (London) **593**, 51 (2021).
[30] A. Crivellin, M. Hoferichter, C. A. Manzari, and M. Montull, Phys. Rev. Lett. **125**, 091801 (2020).
[31] A. Keshavarzi, W. J. Marciano, M. Passera, and A. Sirlin, Phys. Rev. D **102**, 033002 (2020).
[32] G. Colangelo, M. Hoferichter, and P. Stoffer, Phys. Lett. B **814**, 136073 (2021).
[33] R. Aaij *et al.* (LHCb Collaboration), J. High Energy Phys. 08 (2017) 055.
[34] A. Abdesselam *et al.* (Belle Collaboration), Phys. Rev. Lett. **126**, 161801 (2021).
[35] R. Aaij *et al.* (LHCb Collaboration), arXiv:2103.11769.
[36] G. Hiller and F. Kruger, Phys. Rev. D **69**, 074020 (2004).
[37] C. Bouchard, G. P. Lepage, C. Monahan, H. Na, and J. Shigemitsu (HPQCD Collaboration), Phys. Rev. Lett. **111**, 162002 (2013); **112**, 149902(E) (2014).
[38] M. Bordone, G. Isidori, and A. Pattori, Eur. Phys. J. C **76**, 440 (2016).
[39] L. Darmé, M. Fedele, K. Kowalska, and E. M. Sessolo, J. High Energy Phys. 08 (2020) 148.
[40] J. S. Alvarado, S. F. Mantilla, R. Martinez, and F. Ochoa, arXiv:2105.04715.
[41] S. R. Mishra *et al.* (CCFR Collaboration), Phys. Rev. Lett. **66**, 3117 (1991).
[42] M. Bauer, P. Foldenauer, and J. Jaeckel, J. High Energy Phys. 07 (2018) 094.
[43] W. Altmannshofer, S. Gori, J. Martín-Albo, A. Sousa, and M. Wallbank, Phys. Rev. D **100**, 115029 (2019).
[44] M. Davier and H. N. Ngoc, Phys. Lett. B **229**, 150 (1989).
[45] S. Gninenko, N. Krasnikov, and V. Matveev, Phys. Rev. D **91**, 095015 (2015).
[46] J. L. Feng, I. Galon, F. Kling, and S. Trojanowski, Phys. Rev. D **97**, 035001 (2018).
[47] A. Ariga *et al.* (FASER Collaboration), arXiv:1811.10243.
[48] A. Ariga *et al.* (FASER Collaboration), arXiv:1812.09139.
[49] A. Ariga *et al.* (FASER Collaboration), Phys. Rev. D **99**, 095011 (2019).
[50] A. Ariga *et al.* (FASER Collaboration), arXiv:1901.04468.
[51] A. Berlin, S. Gori, P. Schuster, and N. Toro, Phys. Rev. D **98**, 035011 (2018).
[52] C. Aidala *et al.* (SeaQuest Collaboration), Nucl. Instrum. Methods Phys. Res., Sect. A **930**, 49 (2019).
[53] M. Anelli *et al.* (SHiP Collaboration), arXiv:1504.04956.
[54] S. Alekhin *et al.*, Rep. Prog. Phys. **79**, 124201 (2016).
[55] B. Batell, A. Freitas, A. Ismail, and D. Mckeen, Phys. Rev. D **98**, 055026 (2018).
[56] J. P. Leveille, Nucl. Phys. **B137**, 63 (1978).
[57] R. Harnik, J. Kopp, and J. Zupan, J. High Energy Phys. 03 (2013) 026.
[58] V. Ilisie, J. High Energy Phys. 04 (2015) 077.
[59] Z. G. Berezhiani, Phys. Lett. B **129**, 99 (1983).
[60] D. Chang and R. N. Mohapatra, Phys. Rev. Lett. **58**, 1600 (1987).
[61] A. Davidson and K. C. Wali, Phys. Rev. Lett. **59**, 393 (1987).
[62] A. De Pace, H. Muther, and A. Faessler, Phys. Lett. B **188**, 307 (1987).
[63] S. Rajpoot, Mod. Phys. Lett. A **02**, 307 (1987); **02**, 541(E) (1987).
[64] K. S. Babu and R. N. Mohapatra, Phys. Rev. Lett. **62**, 1079 (1989).

[65] K. S. Babu and R. N. Mohapatra, Phys. Rev. D **41**, 1286 (1990).
[66] K. S. Babu, B. Dutta, and R. N. Mohapatra, J. High Energy Phys. 01 (2019) 168.
[67] D. Akimov *et al.* (COHERENT Collaboration), Science **357**, 1123 (2017).
[68] D. Akimov *et al.* (COHERENT Collaboration), 10.5281/zenodo.1228631 (2018).
[69] D. Akimov *et al.* (COHERENT Collaboration), arXiv:1803.09183.
[70] D. Akimov *et al.* (COHERENT Collaboration), Phys. Rev. D **102**, 052007 (2020).
[71] D. Akimov *et al.* (COHERENT Collaboration), Phys. Rev. Lett. **126**, 012002 (2021).
[72] C. Amsler *et al.* (Crystal Barrel Collaboration), Phys. Lett. B **333**, 271 (1994).
[73] C. Amsler *et al.* (Crystal Barrel Collaboration), Z. Phys. C **70**, 219 (1996).
[74] N. Aghanim *et al.* (Planck Collaboration), Astron. Astrophys. **641**, A6 (2020).
[75] R. Harnik, J. Kopp, and P. A. Machado, J. Cosmol. Astropart. Phys. 07 (2012) 026.
[76] J. Redondo, J. Cosmol. Astropart. Phys. 07 (2008) 008.
[77] R. Bollig, W. DeRocco, P. W. Graham, and H.-T. Janka, Phys. Rev. Lett. **125**, 051104 (2020).
[78] D. Croon, G. Elor, R. K. Leane, and S. D. McDermott, J. High Energy Phys. 01 (2021) 107.
[79] B. Dutta, D. Kim, S. Liao, J.-C. Park, S. Shin, and L. E. Strigari, Phys. Rev. Lett. **124**, 121802 (2020).
[80] B. Aubert *et al.* (*BABAR* Collaboration), Phys. Rev. Lett. **103**, 081803 (2009).
[81] J. Lees *et al.* (*BABAR* Collaboration), Phys. Rev. Lett. **113**, 201801 (2014).
[82] E. Riordan *et al.*, Phys. Rev. Lett. **59**, 755 (1987).
[83] J. Bjorken, S. Ecklund, W. Nelson, A. Abashian, C. Church, B. Lu, L. Mo, T. Nunamaker, and P. Rassmann, Phys. Rev. D **38**, 3375 (1988).
[84] J. D. Bjorken, R. Essig, P. Schuster, and N. Toro, Phys. Rev. D **80**, 075018 (2009).
[85] C.-N. Yang, Phys. Rev. **77**, 242 (1950).
[86] S. Chang, J. Liu, A. Pierce, N. Weiner, and I. Yavin, J. Cosmol. Astropart. Phys. 08 (2010) 018.
[87] J. L. Feng, J. Kumar, D. Marfatia, and D. Sanford, Phys. Lett. B **703**, 124 (2011).
[88] J. L. Feng, J. Kumar, and D. Sanford, Phys. Rev. D **88**, 015021 (2013).
[89] A. H. Abdelhameed *et al.* (CRESST Collaboration), Phys. Rev. D **100**, 102002 (2019).
[90] T. Bringmann and M. Pospelov, Phys. Rev. Lett. **122**, 171801 (2019).
[91] J. B. Dent, B. Dutta, J. L. Newstead, and I. M. Shoemaker, Phys. Rev. D **101**, 116007 (2020).
[92] Z. Z. Liu *et al.* (CDEX Collaboration), Phys. Rev. Lett. **123**, 161301 (2019).
[93] L.-S. Geng, B. Grinstein, S. Jäger, S.-Y. Li, J. M. Camalich, and R.-X. Shi, Phys. Rev. D **104**, 035029 (2021).
[94] R. Aaij *et al.* (LHCb Collaboration), Phys. Rev. Lett. **113**, 151601 (2014).
[95] R. Aaij *et al.* (LHCb Collaboration), Phys. Rev. Lett. **122**, 191801 (2019).
[96] A. Datta, J. Kumar, J. Liao, and D. Marfatia, Phys. Rev. D **97**, 115038 (2018).
[97] W. Altmannshofer, M. J. Baker, S. Gori, R. Harnik, M. Pospelov, E. Stamou, and A. Thamm, J. High Energy Phys. 03 (2018) 188.
[98] W. Altmannshofer and P. Stangl, Eur. Phys. J. C **81**, 952 (2021).
[99] A. Carvunis, F. Dettori, S. Gangal, D. Guadagnoli, and C. Normand, J. High Energy Phys. 12 (2021) 078.
[100] M. Santimaria, New results on theoretically clean observables in rare B-meson decays from LHCb (2021).
[101] M. Aaboud *et al.* (ATLAS Collaboration), J. High Energy Phys. 04 (2019) 098.
[102] A. M. Sirunyan *et al.* (CMS Collaboration), J. High Energy Phys. 04 (2020) 188.
[103] X. He, G. C. Joshi, H. Lew, and R. Volkas, Phys. Rev. D **43**, R22 (1991).
[104] X.-G. He, G. C. Joshi, H. Lew, and R. Volkas, Phys. Rev. D **44**, 2118 (1991).
[105] O. Lutz *et al.* (Belle Collaboration), Phys. Rev. D **87**, 111103 (2013).
[106] P. Ball and R. Zwicky, Phys. Rev. D **71**, 014029 (2005).
[107] W. Cheng, X.-G. Wu, and H.-B. Fu, Phys. Rev. D **95**, 094023 (2017).
[108] A. Khodjamirian, T. Mannel, A. A. Pivovarov, and Y. M. Wang, J. High Energy Phys. 09 (2010) 089.
[109] J. P. Lees *et al.* (*BABAR* Collaboration), Phys. Rev. D **87**, 112005 (2013).
[110] D. M. Straub, arXiv:1810.08132.
[111] J. Grygier *et al.* (Belle Collaboration), Phys. Rev. D **96**, 091101 (2017); **97**, 099902(A) (2018).
[112] R. Aaij *et al.* (LHCb Collaboration), J. High Energy Phys. 05 (2013) 159.
[113] R. Aaij *et al.* (LHCb Collaboration), J. High Energy Phys. 06 (2014) 133.
[114] R. Aaij *et al.* (LHCb Collaboration), J. High Energy Phys. 09 (2015) 179.
[115] R. Aaij *et al.* (LHCb Collaboration), J. High Energy Phys. 06 (2015) 115; 09 (2018) 145(E).
[116] R. Aaij *et al.* (LHCb Collaboration), J. High Energy Phys. 10 (2020) 156.
[117] R. Aaij *et al.* (LHCb Collaboration), Phys. Rev. Lett. **122**, 191801 (2019).
[118] R. Aaij *et al.* (LHCb Collaboration), J. High Energy Phys. 12 (2020) 081.
[119] A. Angelescu and P. Huang, Phys. Rev. D **99**, 055023 (2019).
[120] J. Ellis, Comput. Phys. Commun. **210**, 103 (2017).